Combustion and Flame 157 (2010) 1111–1121

Contents lists available at ScienceDirect

Combustion and Flame

journal homepage: www.elsevier.com/locate/combustflame

A dynamic multi-timescale method for combustion modeling with detailed and reduced chemical kinetic mechanisms

Xiaolong Gou [a,b], Wenting Sun [a], Zheng Chen [a,c], Yiguang Ju [a,*]

[a] Department of Mechanical and Aerospace Engineering, Princeton University, NJ 08544, USA
[b] College of Power Engineering, Chongqing University, Chongqing 400030, China
[c] School of Engineering, Peking University, Beijing 100871, China

ARTICLE INFO

Article history:
Received 30 July 2009
Received in revised form 1 September 2009
Accepted 23 February 2010
Available online 16 March 2010

Keywords:
Multi-timescale modeling
Reduced kinetic mechanisms
Multi-scale
n-Decane ignition

ABSTRACT

A new on-grid dynamic multi-timescale (MTS) method is presented to increase significantly the computation efficiency involving multi-physical and chemical processes using detailed and reduced kinetic mechanisms. The methodology of the MTS method using the instantaneous timescales of different species is introduced. The definition of the characteristic time for species is examined and compared with that of the computational singular perturbation (CSP) and frozen reaction rate methods by using a simple reaction system. A hybrid multi-timescale (HMTS) algorithm is constructed by integrating the MTS method with an implicit Euler scheme, respectively, for species with and without the requirement of accurate time histories at sub-base timescales. The efficiency and the robustness of the MTS and HMTS methods are demonstrated by comparing with the Euler and VODE solvers for homogenous ignition and unsteady flame propagation of hydrogen, methane, and *n*-decane–air mixtures. The results show that both MTS and HMTS reproduce well the species and temperature histories and are able to decrease computation time by about one-order with the same kinetic mechanism. Compared to MTS, HMTS has slightly better computation efficiency but scarifies the stability at large base time steps. The results also show that with the increase of mechanism size and the decrease of time step, the computation efficiency of multi-timescale method increases compared to the VODE solver. In addition, it is shown that the integration of the multi-timescale method with the path flux analysis based mechanism reduction approach can further increase the computation efficiency. Unsteady simulations of outwardly propagating spherical *n*-decane–air premixed flames demonstrate that the multi-timescale method is rigorous for direct numerical simulations with both detailed and reduced chemistry and can dramatically improve the computation efficiency.

1. Introduction

Recent concerns over energy sustainability, energy security, and global warming have presented grand challenges to develop non-petroleum based low carbon fuels and advanced engines to achieve improved energy conversion efficiency and reduced emissions [1,2]. Transportation contributes to about one-third of the global carbon emissions. Therefore, it is urgently needed to develop alternative fuels and predictive combustion modeling capabilities to optimize the design and operation of advanced engines for transportation applications.

Combustion is a multi-scale physical and chemical process. It involves various time and length scales ranging from atomic excitation to turbulent transport [3]. Even with the availability of high-performance supercomputing capability at petascale and beyond, the multi-physics and multi-timescale nature of combustion processes remain to be a great challenge to direct numerical simulations of practical reaction systems [4].

At first, the kinetic mechanisms for hydrocarbon and synthetic bio-fuels typically consist of tens to hundreds of species and hundreds to thousands of reactions. The large number of reactive species requires an enormous computation power and data storage capacity. It has been shown that even with a simple mechanism the majority of the CPU time for a CFD simulation is spent on the computation of the chemistry and species diffusion [5]. It is well known that the CPU time of a typical full Jacobian matrix decomposition based implicit algorithm (e.g. a stiff ordinary differential equation solver (VODE) [6]) is proportional to the cube of the species number. The ratio of computing time for reactions will become even larger as the size of the mechanism increases. Secondly, the broad range of length and timescales of transport and kinetic reactions create problems of grid resolution and stiffness in direction numerical simulation. An explicit algorithm such as the Euler

* Corresponding author. Fax: +1 609 258 6233.
E-mail address: yju@princeton.edu (Y. Ju).

0010-2180/$ - see front matter © 2010 The Combustion Institute. Published by Elsevier Inc. All rights reserved.
doi:10.1016/j.combustflame.2010.02.020

scheme will have to use the smallest timescale based on the finest grid and fastest reaction group [6, 7], leading to a dramatic increase of computation time. Thirdly, the multi-physical non-linear coupling between continuum regime (e.g. flow with small concentration/temperature gradients) and non-continuum regime (e.g. particle and molecular dynamics) and the statistical coupling between mean values and sub-grid statistical values requires accurate resolutions of the time histories of variables with different time and length scales (Fig. 1). For an example, a nanosecond non-equilibrium plasma assisted combustion needs to calculate electron energy distributions and quenching of excited species in nanoseconds and combustion in a few seconds.

In order to make numerical simulations of reactive flow computationally affordable, various mechanism reduction methods have been developed to generate reduced kinetic mechanisms by decreasing the number of species while keeping the mechanism reasonably comprehensive [5]. The first approach for reducing the mechanism size is the sensitivity and rate analysis [8–10]. Although this method is very effective in generating compact reduced mechanisms, it provides neither the timescales of different reaction groups nor the possible quasi-steady state (QSS) species and partial equilibrium groups without good human experience. The second approach is the reaction Jacobian analysis which includes the computational singular perturbation (CSP) method [11–13] and the Intrinsic Low Dimensional Manifold (ILDM) [14]. This approach can effectively identify the timescales of different reaction groups, QSS species, or low dimensional manifolds. However, it requires significant computation time to conduct Jacobian decomposition and mode projection. This type of method is therefore not suitable to be used in direct numerical simulation. To achieve more efficient calculations of fast mode species, a third approach, the parameterization method, was proposed. The In Situ Adaptive Tabulation (ISAT) [15], Piecewise Reusable Implementation of Solution Mapping (PRISM) [16], High Dimensional Model Representation (HDMR) [17], and polynomial parameterizations [18] are the typical examples of this category. However, for non-premixed turbulent combustion involving a large kinetic mechanism with a broad temperature distribution, the constraints for validity of low dimensional manifolds, large time consumption in table buildup, and the difficulties in data retrieval from table look-up lead to decreased advantage of ISAT in comparison to direct integration [19]. In order to achieve efficient reaction model reduction, a fourth method is presented to use the reaction rate or reaction path relations as a measure of the degree of interaction among species. Bendsten et al. [20] adopts a reaction matrix (P) with each of whose elements P_{ij} defined as the net production rate of species i from all reactions involving j to establish a skeletal reaction path way (or mechanism). The set of important species is selected by going through the reaction matrix following the path that connects one species to another that is most strongly coupled with it. The skeletal mechanism is then completed by including a number of reactions such that for each of the selected species, a certain percentage of the total production or consumption rate (threshold value) of that species is kept in the skeletal mechanism. Similar strategies are used in the Directed Relation Graph (DRG) method [21], the Directed Relation Graph method with Error Propagation (DRGEP) [22], and the path flux analysis method [23]. Although the DRGEP and PFA methods considerably improve the effectiveness of mechanism reduction, the size of reduced mechanism for a typical jet fuel surrogate is still too large to be used directly in large scale numerical simulations.

Recently, it has been recognized that no matter what kind of mechanism reduction methods discussed above are used, the size of the reduced comprehensive mechanisms capable to reproduce low temperature ignition delay time remain very large. Although the introduction of QSS and sensitivity analysis can remove further a few species, the validity of QSS assumption for a given species is questionable in the entire simulation domain where temperature and pressure are beyond the pre-specified QSS conditions due to turbulent transport. Recently, although the on-the-fly QSS assumption can be used to resolve the issue of the QSS assumption, rigorous selection and efficient solution of QSS species remain as a challenging issue [4,5]. More importantly, when the transient information of short timescales is needed for the modeling of physical processes in larger timescales in a multi-physics problem, the application of the on-the-fly QSS is also limited.

Therefore, the question becomes: are there any simple and alternative methods which can efficiently integrate a multi-timescale problem and retain the transient information of species and physical processes at different timescales. A convenient way to obtain time accurate solution of various reaction groups is the Euler method. However, an explicit Euler method needs a time-marching step smaller than the smallest timescale in a physical process [7]. For stiff combustion processes, the smallest timescale can be 10^{-12} s or smaller, which makes the explicit Euler method only limited to small scale direct numerical simulations. To resolve

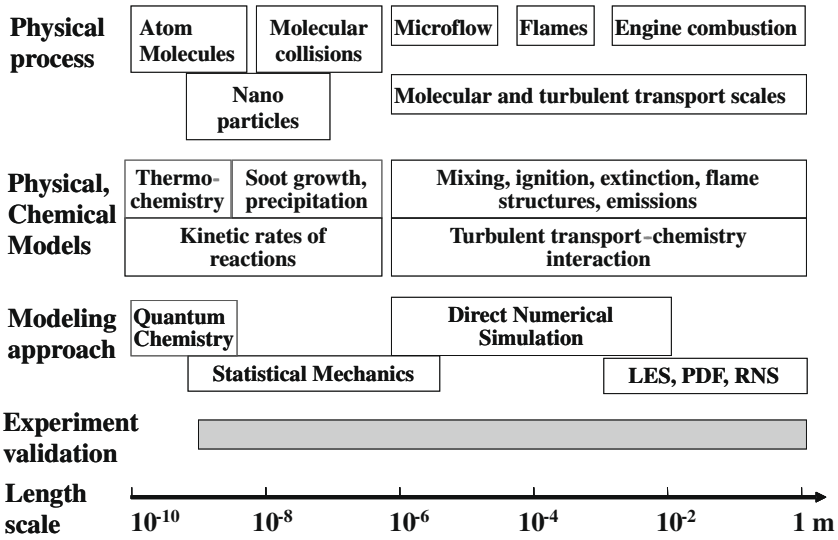

Fig. 1. Multi-scale nature of combustion process with a detailed kinetic mechanism.

the stiffness of combustion problems, an implicit approach such as the ordinary differential equation (VODE) solver [6,24–26] is often used. Curtiss and Hirschfelder [25] and Gear [26] provided the first pragmatic definition of stiff equations as those for which certain implicit methods, particularly backward difference formulas (BDF), perform better than explicit ones. The VODE solver [6] is popularly utilized in the combustion community to handle detailed chemistry. However, for an unsteady problem, an implicit solver for detailed chemistry is often computationally expensive, even for the simulation of one-dimensional propagating spherical methane/air flames with detailed chemistry [27]. The situation becomes even worse for large hydrocarbons which have hundreds of species in the oxidation mechanisms. More importantly, when an implicit VODE solver is used, the time histories of species and variables with fast timescales are lost although many fast variables in combustion change smoothly. Therefore, in addition to the need of development of a rigorous kinetic mechanism reduction method, it is also necessary to develop an efficient, robust, and accurate numerical method which can retain the time-accurate information of variables of fast timescales for a stiff and multi-physics reactive flow.

Recently, several different multi-scale methods have been developed for numerical integration of stiff ODEs. For example, the heterogeneous multi-scale method (HMM) [28,29] is a general framework for the numerical approximation of multi-timescale problems and was developed for solving ODEs containing different timescales [30,31]. Savcenco et al. [32] proposed a multirate time stepping method by using prediction and time dividing and demonstrated an improved computation efficiency for stiff ODEs. However, this approach does not suit for combustion modeling with a detailed mechanism in which the timescales range several orders. A new strategy to predict the timescales and to avoid the full integration of ODEs at the smallest time step is necessary. To the authors' knowledge, there have been no studies of multi-timescale methods for any realistic chemical kinetic reactions.

In this paper, we present a dynamic multi-timescale method (MTS) and a hybrid multi-timescale method (HMTS) for the modeling of unsteady reactive flow with both detailed and reduced kinetic mechanisms of hydrocarbon fuels and to demonstrate the improved computation efficiency and robustness. In the following, at first, the mathematical models of MTS and HMTS methods will be introduced. Secondly, a comparison of the characteristic time for species predicted by the present method, the CSP projection method, and the frozen reaction rate method will be made using a simple reaction system. Thirdly, the computation efficiency and accuracy of the MTS and HMTS methods will be demonstrated through the comparisons with the conventional Euler and VODE solvers from the simulations of auto-ignition of hydrogen, methane, and *n*-decane/air mixtures with detailed mechanisms. Finally, the multi-timescale method is used to simulate unsteady spherical flame propagation of the *n*-decane–air mixtures with both reduced and detailed mechanisms. The increased robustness and computation efficiency of the present method for the modeling of unsteady propagating flames with both detailed and reduced mechanisms are demonstrated.

2. The multi-timescale method

In recent years, on-grid operator-splitting schemes have been used in reactive flow simulations and the stiff source term due to chemical reactions are treated by the so called point implicit or fractional-step procedure [33,34]. In this method, for a given time step, on each grid a non-reaction flow is solved in the first fractional step and the stiff ODEs associated with detailed chemical reactions are solved in the second fractional step for a homogeneous reaction system. The present study is to develop an efficient and accurate MTS and HMTS algorithms to integrate the stiff ODEs on each computation grid with detailed and reduced kinetic mechanisms.

To demonstrate the multi-timescale nature of a reactive flow with detailed chemistry, in this study, homogenous ignition of hydrogen/air, methane/air and *n*-decane/air at a constant pressure is simulated. For hydrogen/air combustion, the C_1 mechanism [35] is employed. For methane/air mixtures, the GRI-MECH 3.0 mechanism [36] of 53 species and 325 reactions is used. For *n*-decane/air mixtures, the high temperature mechanism for surrogate jet fuels [37] which consists of 121 species and 866 reactions is utilized. Fig. 2 show the timescales of species during homogeneous ignition of the stoichiometric *n*-decane/air mixture initially at $T = 1400$ K and $P = 1$ atm at $t = 0.1$, 0.2, and 0.3 ms, respectively. Before the thermal runaway, for example, at $t = 0.1$ ms, the characteristic times for most species estimated by using the present definition (Eq. (5) in the next section) are in the range of 10^{-4}–10^{-10} s. However, after the thermal runaway, for example, at $t = 0.2$ or 0.3 ms, the range of timescale distribution changes to 10^{-7}–10^{-13} s. It is confirmed that an explicit Euler integration of the ODEs will not be able to converge unless the time step is about 10^{-13} ns. Therefore, the reactive system is intrinsically dynamic and multi-timescale and the characteristic time of different species spans a wide range, leading to the difficulty of the conventional explicit Euler solver and the QSS assumption for any pre-specified species.

In order to efficiently solve the multi-timescale problem in a reactive flow without introducing pre-specified QSS assumptions and keeping the simplicity of the Euler scheme, we will present here a multi-timescale (MTS) method. The basic idea of the multi-timescale (MTS) method is shown in Fig. 3a. First of all, in each simulation a base time step, t_{base}, is specified based on the interest of the physical problem and the information needed at sub-time scale to construct models at the physical timescale of interest. Then, based on the base time step and the estimated characteristic time of each species (note that as described in the following section, this present scheme does not need an accurate estimation of the characteristic time of species), all the species will be divided into different groups according to their timescales. At each time step of t_{base}, from the fastest group (Δt_F) to the slowest group (Δt_S), all the groups are calculated with their own time steps by using a first-order explicit Euler scheme until a converging criterion with both absolute and relative errors is met. The first-order Euler scheme has an accuracy of $O(\Delta t)$ and can be easily

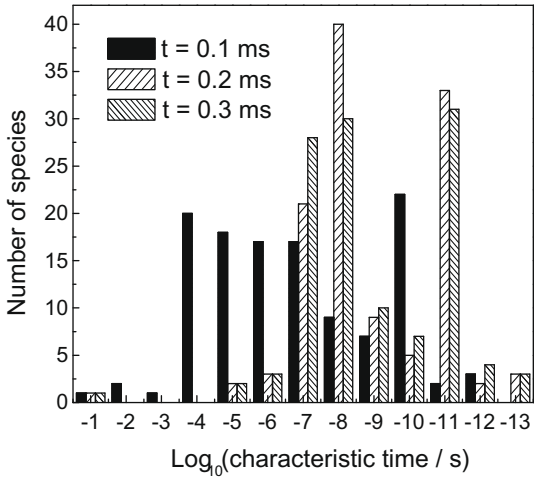

Fig. 2. Characteristic timescale of species for homogeneous *n*-decane ignition at time of 0.1, 0.2, and 0.3 ms, respectively.

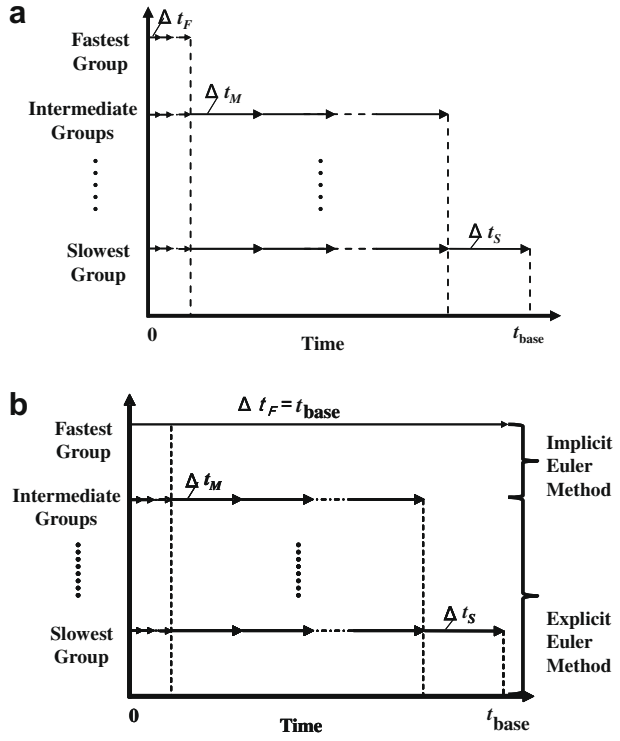

Fig. 3. (a) Diagram of multi-timescale (MTS) method. Δt_F is the time step of the fastest group, Δt_M is the time step of an intermediate group, Δt_S is the time step of the slowest group, and t_{base} is the base time step. (b) Diagram of hybrid multi-timescale (HMTS) method. Δt is the time step of the fastest group, Δt_M is the time step of an intermediate group, Δt_S is the time step of the slowest group, and t_{base} is the base time step.

parallelized on each grid. Note that by using a Runge–Kutta method, higher-order schemes can be constructed [7,27].

In some cases such as high temperature ignition, one only has interest in the phenomena of large timescales and the transient time histories of certain physical processes or reaction groups may not be needed. Therefore, time accurate integration for the short timescale species or groups by using an explicit Euler scheme is not necessary and a larger time step together with an implicit Euler scheme can be applied more efficiently. As shown in Fig. 3b, for example, if the time histories of the fast groups are not needed, the integration of these selected groups will be replaced by using an implicit Euler scheme. For the rest of groups, the explicit Euler scheme is still applied. This algorithm is called the hybrid multi-timescale (HMTS) method. It combines the explicit Euler scheme with an implicit Euler scheme for integration of species with short characteristic time. Note that, the selection of the implicit Euler scheme for species groups is not limited by the timescale, but by the interest of the need for accurate time history of the reaction groups.

In the MTS method, the time step for integrating each species group has to be smaller than the characteristic time of any species in this group to ensure the convergence of the explicit Euler method [7]. At the same time, although it is necessarily to be accurate but needs to be closer to the true local timescale so that the computation efficiency can be maximized. However, for HMTS, the groups which use the implicit Euler method will be integrated by using the base time step (t_{base}) directly.

In the following, we briefly summarize the implementation of the on-grid dynamic MTS and HMTS methods for combustion modeling involving detailed or reduced kinetic mechanisms. For example, for an adiabatic and homogeneous system on each computation grid, the governing equations for mass conservation and energy conservation in an adiabatic and constant pressure process can be written as,

$$\frac{dY_i}{dt} = \omega_i(T, Y_1, Y_2, \ldots Y_{NS})W_i/\rho, \tag{1}$$

$$\frac{dT}{dt} = -\sum_{i=1}^{II} h_i\omega_i(T, Y_1, Y_2, \ldots Y_{NS})/\rho c_p \tag{2a}$$

or

$$h(T, Y_1, Y_2, \ldots Y_{NS}) = h^0 \tag{2b}$$

where t is the time, T the temperature, ρ the density, and c_p is the heat capacity. Y_i, ω_i, and h_i are, respectively, the mass fraction, the net production rate, and the enthalpy of species i. Ns is the total number of species. For a constant volume process, the energy equation can be replaced by the conservation of the internal energy,

$$e(T, Y_1, Y_2, \ldots Y_{NS}) = e_0 \tag{3}$$

where e_0 is the initial internal energy per unit volume of the mixture.

In the conventional Euler method, the conservation equations are solved explicitly by using a single time step smaller than the minimum characteristic time of all species. Although the Euler method is widely used in direct numerical simulations, the computation efficiency is very low due to the strong constraint in time step [7]. As shown in Fig. 2, in order to calculate the ignition of n-decane, the time step for the explicit Euler method has to be smaller than 10^{-13} s. On the other hand, in an implicit method such as the VODE solver [6], the governing equation is solved implicitly by using a Jacobian decomposition. As shown below, although this approach is robust for larger time steps, the computation efficiency using this method for unsteady flow simulations is very low because of the huge cost of matrix inversion.

In the MTS method, as shown in Fig. 3a, unlike the conventional Euler method, the conservation equations for all species are integrated with their own characteristic timescales. In order to find the characteristic time of each species, the net production rate, ω_k, in the governing equation of each species can be divided into two parts, a creation rate, C_k, and a destruction rate, D_k,

$$\frac{dY_k}{dt} = C_k(T, \rho, Y_1, Y_2, \ldots Y_{k-1}, Y_{k+1}, \ldots Y_{NS}) - D_k(T, \rho, Y_1, Y_2, \ldots Y_{NS}) \tag{4}$$

where

$$D_k(T, \rho, Y_1, Y_2, \ldots Y_{NS}) = Y_k^l F_k(T, \rho, Y_1, Y_2, \ldots Y_{k-1}, Y_{k+1}, \ldots Y_{NS}), \quad l \geqslant 1$$

All the reactions involving the participation of the kth species as a reactant are included in D_k. From a linear analysis, a characteristic time, τ_k, for the destruction of species k can be approximately estimated as,

$$\tau_k = -\left[\frac{\partial}{\partial Y_k}\left(\frac{dY_k}{dt}\right)\right]^{-1} = \left(\frac{\partial D_k}{\partial Y_k}\right)^{-1} \tag{5}$$

A further discussion of the validity of the definition of characteristic time of species in Eq. (5) will be made in the following section by using a skeletal reaction scheme.

In the numerical simulation process, the base time step t_{base} is chosen from the interest of the physical phenomenon (e.g. turbulent mixing, transient ignition, or plasma discharge). At the same time, the characteristic time of all species can be estimated from Eq. (5). Since many species may have the same or similar timescales, these species can be grouped as one integration group. By defining that each neighboring group has a difference of timescale

in one-order, the number of timescale groups, N_m, and the group index of the kth species N_k can be obtained as,

$$N_m = \left\lfloor Log_{10}\left(\frac{\Delta t_{base}}{\tau_{\min}}\right)\right\rfloor + 1 \tag{6}$$

$$N_k = \left\lfloor Log_{10}\left(\frac{\Delta t_{base}}{\tau_k}\right)\right\rfloor + 1 \tag{7}$$

Note that the member of groups and the number of groups are varied at each base time step and grid in order to include the rapid change of the characteristic time of certain species. Therefore, for example, for a constant pressure system the species in the Nth group will be solved explicitly using the characteristic time of Nth group by using,

$$Y_k^{n+1,m+1} = Y_k^{n+1,m} + \Delta t_n \frac{\omega_k W_k}{\rho} \tag{8}$$

$$T^{n+1,m+1} = T^{n+1,m} + \Delta t_n \left(\frac{-\sum_{i=1}^{II} h_i \omega_i W_i}{\rho c_p}\right) \tag{9}$$

where W_i is the molecular weight of the ith species. The superscript and subscript n means the nth time step, and m is the mth iteration. Normally, for Euler integrations of each group, only a few steps (e.g. 4–5 steps) are needed to meet the convergence criteria (an absolute error of ATOL = 1.0×10^{-13} and a relative error of RTOL = 1.0×10^{-4}). Note that to improve the accuracy, in the integration of the faster modes, the slower modes are updated as well. The values of the converged fast groups are then fixed until the convergence of all the slow species is reached at the end of the base time step. Therefore, MTS has a similar form to the conventional explicit Euler method except that each species in different groups is integrated with a different time step. In fact, in the limiting case when all species are integrated at the smallest time step, MTS method automatically reduces to the conventional Euler method. However, as shown later, MTS allows integration of a much larger base time step and is more robust and computationally efficient than the conventional Euler method.

In the HMTS method, the species selected for implicit integration are solved by using an iterative implicit Euler scheme. In this method, by using Eqs. (2) and (4) the species iteration and energy equation for a constant pressure system is written as,

$$\begin{aligned} &Y_k^{n+1,m+1} = (Y_k^n + \Delta t C_k^{n+1,m})/(1 + \Delta t E_k^{n+1,m}) \\ &h(T^{n+1}, Y_1^{n+1}, Y_2^{n+1}, \ldots Y_{NS}^{n+1}) = h^0 \end{aligned} \tag{10}$$

where $E_k = D_k/Y_k$. At a given time step of n, the species in Eq. (10) are solved iteratively until the convergent thresholds ATOL and RTOL are met. After the initial implicit steps for hybrid species, the MTS method will continue to integrate the governing equation to the specified based time step. Therefore, HMTS is a two-step approach. In one limit, if no group is chosen to be solved implicitly, it reduces to the MTS method. In the other limit, if all groups are chosen to be solved implicitly, it becomes a fully implicit method. Therefore, the HMTS is a general method which includes Euler, MTS, and the fully implicit methods in three limiting cases, respectively. In the following comparisons between MTS, HMTS, and the VODE solver, the same base time step and relative and absolute error thresholds are used for all schemes. In the VODE solver, the first-order time integration and numerical Jacobian are employed.

3. Results and discussion

3.1. Comparison of the estimations of species timescale

In the present multi-timescale method, as shown in Eq. (5), we need to define a characteristic time for each species for the explicit Euler integration. Unfortunately, strictly speaking, although the characteristic time of each independent reaction mode can be determined from the CSP analysis, the characteristic time of each species does not exist because each species is involved in several independent modes. Fortunately, our method does not require an accurate determination of the timescales of species. Instead, only an approximate timescale is needed for the purpose of the efficient and convergent integration of the explicit Euler method at a small integration time step. Of course, a better determination of the characteristic time of species will increase the computation efficiency. In the following, we will use a simple example to demonstrate the effectiveness of timescale estimation in Eq. (5) by comparing it with the CSP method and the "frozen" reaction rate representation method.

We first discuss the estimation of species timescale by using the CSP method. For a reactive system with Ns species, there exist Ns linearly independent or conjugate reaction modes, and the timescales for all reaction modes can be determined from the eigen-values of the reaction Jacobian [11,13]. A pair of conjugate modes will involve two coupled reaction modes with the same oscillatory and growth or decay timescales. The timescale of each reaction group can be obtained by using the CSP method. By using a species vector, $\mathbf{y}$, and the reaction vector $\boldsymbol{\omega}$, Eq. (1).can be rewritten as

$$\mathbf{g}(\mathbf{y}) \equiv \frac{d\mathbf{y}}{dt} = \omega = \mathbf{S} \cdot \mathbf{F}(\mathbf{y}) \tag{11}$$

where $\mathbf{S}$ and $\mathbf{F}(\mathbf{y})$ the stoichiometric coefficient matrix and the rate vector of elementary reactions, respectively, and $\boldsymbol{\omega}$ is the mass production rate weighted by density. By taking a time derivative of Eq. (11), we can obtain

$$\frac{d\mathbf{g}}{dt} = \mathbf{J} \cdot \mathbf{g} \tag{12}$$

where $\mathbf{J} = d\mathbf{g}/d\mathbf{y}$ is the time-dependent Jacobian matrix with all real components. Assuming $\mathbf{J}$ is a constant in a small time interval and using the decomposition of $\mathbf{J} = \mathbf{A}\boldsymbol{\Lambda}\mathbf{B}$, the time evolution of each reaction mode, $\mathbf{f}$, can be given as

$$\frac{d\mathbf{f}}{dt} = \boldsymbol{\Lambda}\mathbf{f}, \quad f \equiv \mathbf{Bg} \tag{13}$$

where $\mathbf{A}$ is the matrix of basis vectors and $\mathbf{B}$ is the inverse matrix of $\mathbf{A}$. In Eq. (13), if $\mathbf{A}$ is an ideal basis matrix, $\boldsymbol{\Lambda}$ reduces to a diagonal matrix and its Ns diagonal elements are the eigen-values (λ_k) of the Ns reaction modes. The timescale of each reaction mode is the inverse of the corresponding eigenvalue,

$$\tau_k \equiv 1/\lambda_k \tag{14}$$

To estimate the characteristic time of a species, Lam [11] proposed using a radical pointer based on the Ns diagonal elements of the projection matrix of each species to the mth reaction mode,

$$\mathbf{Q_m} = \mathbf{Diag}[\mathbf{a_m} \bullet \mathbf{b^m}] \tag{15}$$

By extending the concept of radical pointer, the characteristic time of the $k$ith species can be approximately defined as [13],

$$\tau_k \equiv 1 \Big/ \sum_{m=1}^{N} Q_m(k)\lambda_m \tag{16}$$

Unfortunately, the calculations of the reaction Jacobin, eigenvalues, and the projection matrix at each time step and on each grid point are computationally expensive. It is not realistic to use Eq. (16) to estimate the characteristic time of species in the present multi-timescale method.

An alternative and simplest approximation of the reaction timescale of the kth species in a reaction system is using the reaction rate directly [38],

$$\tau_k = Y_k \Big/ \left|\left(\frac{dY_k}{dt}\right)\right| = Y_k \Big/ |\omega_k W_k/\rho| \tag{17}$$

However, this approximation is based on a global "frozen" reaction rate representation and ignores the dynamic equilibrium of the chemical reactions. As a result, all species timescales become to infinity at chemical equilibrium conditions (zero net reaction rate). This is not reasonable because even at equilibrium conditions, each species still has a finite timescale involving in a dynamic chemical equilibrium. A small perturbation will drive each species to move away from the equilibrium state at that timescale.

In this study, as shown in Eq. (5), we use the gradient of the species consumption rate in the species coordinate to define the species timescale,

$$\tau_k = -\left[\frac{\partial}{\partial Y_k}\left(\frac{dY_k}{dt}\right)\right]^{-1} = Y_k \Big/ \sum_{i=1}^{II} \nu_{ki} D_{ki}(T, Y_1, Y_2, \ldots Y_{NS}) \tag{18}$$

For most elementary reactions, each species only involves in reactions with other species. In this case ($\nu_k = 1$), the timescale can be estimated as,

$$\tau_k = Y_k / D_k(T, Y_1, Y_2, \ldots Y_{NS}) \tag{19}$$

Eq. (19) is consistent with the definition of the lifetime of species given in [39]. In fact, our simulation shows that the MTS and HMTS work well for both Eqs. (18) and (19), implying that the estimation of species timescale does not need to be accurate.

To compare the above three methods and demonstrate the effectiveness of the present method for the estimation of the characteristic time of species, we consider the following simple (first-order) reaction system from species A to species B and C: $A \xrightarrow{K_1} C$, $B \xrightarrow{K_2} C$, and $C \xrightarrow{K_3} B$. The ordinary differential equations and the initial boundary conditions can be written as

$$\mathbf{g} \equiv \frac{d}{dt}\begin{pmatrix} Y_A \\ Y_B \\ Y_C \end{pmatrix} = \begin{bmatrix} -k_1 & 0 & 0 \\ 0 & -k_2 & k_3 \\ k_1 & k_2 & -k_3 \end{bmatrix} \begin{pmatrix} Y_A \\ Y_B \\ Y_C \end{pmatrix},$$

$$\text{with} \begin{pmatrix} Y_A \\ Y_B \\ Y_C \end{pmatrix} \Big/ \Big|_{t=0} = \begin{pmatrix} 1 \\ 0 \\ 0 \end{pmatrix} \tag{20}$$

The exact solutions for the mass fractions of A, B, and C are, respectively,

$$Y_A(t) = e^{-k_1 t},$$

$$Y_B(t) = \frac{k_3}{k_2 + k_3} + \frac{k_3}{k_1 - k_2 - k_3} e^{-k_1 t} - \left(\frac{k_3}{k_2 + k_3} + \frac{k_3}{k_1 - k_2 - k_3}\right) e^{-(k_2 + k_3)t}, \tag{21}$$

$$Y_C(t) = 1 - [Y_A(t) + Y_B(t)]$$

From the CSP method, the reaction Jacobian and the matrix of base vectors are given as,

$$\mathbf{J} = \frac{d\mathbf{g}}{dY} = \begin{bmatrix} -K_1 & 0 & 0 \\ 0 & -K_2 & K_3 \\ K_1 & K_2 & -K_3 \end{bmatrix} = \mathbf{A}\mathbf{\Lambda}\mathbf{B} \tag{22}$$

where

$$\mathbf{\Lambda} = \begin{bmatrix} -K_2 - K_3 & 0 & 0 \\ 0 & -K_1 & 0 \\ 0 & 0 & 0 \end{bmatrix}, \quad A = \begin{bmatrix} 0 & \frac{K_1 - K_2 - K_3}{K_3} & 0 \\ -1 & 1 & \frac{K_3}{K_2} \\ 1 & \frac{K_2 - K_1}{K_3} & 1 \end{bmatrix},$$

$$\text{and } B = \begin{bmatrix} \frac{K_1 K_3}{(K_1 - K_2 - K_3)(K_2 + K_3)} & \frac{-K_2}{K_2 + K_3} & \frac{K_3}{K_2 + K_3} \\ \frac{K_3}{K_1 - K_2 - K_3} & 0 & 0 \\ \frac{K_2}{K_2 + K_3} & \frac{K_2}{K_2 + K_3} & \frac{K_2}{K_2 + K_3} \end{bmatrix} \tag{23}$$

The diagonal elements in $\mathbf{\Lambda}$ denote the eigen-values of the following three reaction modes,

$$f_1 = \frac{K_3 K_1 Y_A}{K_3 + K_2 - K_1} + K_2 Y_B + K_3 Y_C$$
$$f_2 = \frac{K_3 K_1 Y_A}{K_3 + K_2 - K_1}, \tag{24}$$
$$f_3 = \frac{d(Y_A + Y_B + Y_B)}{dt} = 0$$

The corresponding timescales of the above three modes are, respectively, $1/(K_2 + K_3)$, $1/K_1$, and infinity. The infinity timescale of the third mode comes from the mass conservation of the reaction system. In order to obtain the characteristic time of each species, the radical pointers from the projection matrix of the three reaction modes to three species are obtained from Eq. (15) respectively,

$$\mathbf{Q}_1 = Diag[\mathbf{a}_1 \bullet \mathbf{b}^1] = \left[0, \frac{K_2}{K_2 + K_3}, \frac{K_3}{K_2 + K_3}\right]$$
$$\mathbf{Q}_2 = Diag[\mathbf{a}_2 \bullet \mathbf{b}^2] = [1, 0, 0], \tag{25}$$
$$\mathbf{Q}_3 = Diag[\mathbf{a}_3 \bullet \mathbf{b}^3] = \begin{bmatrix} 0 & \frac{K_3}{K_2 + K_3} & \frac{K_2}{K_2 + K_3} \end{bmatrix}$$

Therefore, by using Eq. (16), the projected timescales for species A, B, and C from the CSP analysis, are, respectively,

$$\tau_A = -1/\{0 \times [-(K_2 + K_3)] + 1 \times (-K_1) + 0 \times 0\} = 1/K_1$$
$$\tau_B = -1/\left\{\frac{K_2}{K_2 + K_3} \times [-(K_2 + K_3)] + 0 \times (-K_1) + \frac{K_3}{K_2 + K_3} \times 0\right\} = 1/K_2 \tag{26}$$
$$\tau_C = -1\left\{\frac{K_3}{K_2 + K_3} \times [-(K_2 + K_3)] + 0 \times (-K_1) + \frac{K_2}{K_2 + K_3} \times 0\right\} = 1/K_3$$

To demonstrate validity of the present method for timescale estimation, the comparison of the timescales predicted by the above different methods using Eqs. (21), (18) and (26) for constant reaction rates at $K_1 = 1$, $K_2 = 10$, and $K_3 = 100$ are shown in Fig. 4. It is seen that the present method predicts the same results as the CSP projected species timescales. In addition, the timescales of species A and B predicted by the present method are also in good agreement with that of the first two CSP modes (Eq. (23)). The timescale of the third mode from CSP is infinity. However, the predicted timescale for the third species in our method is finite, $1/K_3$. The under-estimation of timescale will make the explicit Euler method numerically stable although it may sacrifice some of the computation efficiency. Overall, in this simple reaction system, our definition of the timescales is consistent with the CSP results from matrix decomposition. However, the present method will significantly improve the computation efficiency of the timescales by eliminating the necessity of the reaction Jacobian and its subsequent decomposition. In Fig. 4, it is also seen that the timescales calculated from the global "frozen" reaction rate representation in Eq. (17) are much larger than those predicted by either the CSP method or the present method. Therefore, the use of the timescales defined in Eq. (17) in the multi-timescale method will ren-

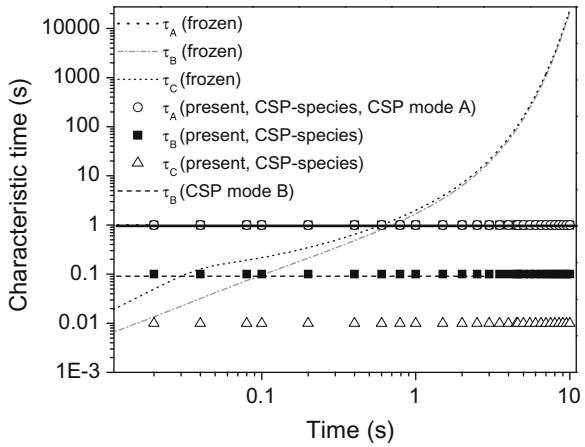

Fig. 4. Comparisons of timescales estimated by using the CSP reaction modes, CSP radical pointer for species, the frozen reaction rate method, and the present method.

der the numerical simulation unstable. The divergence of MTS due to over-estimated timescales using Eq. (17) is confirmed in our numerical simulation.

3.2. Validation of MTS and HMTS for homogeneous ignition systems

The MTS/HMTS methods described above were tested and compared with the explicit Euler and the implicit VODE solvers [6] for homogeneous ignition and unsteady spherical flame propagation in *n*-decane, methane, hydrogen–air mixtures. The relative and absolute error thresholds (**RTOL** and ATOL) for VODE and MTS/HMTS are, respectively, 1×10^{-4} and 1×10^{-13}. Unless otherwise stated, in the calculations of the HMTS method, only the fastest one group was chosen for the implicit method.

Fig. 5 shows the comparison of the temperature, major species, and radical concentrations calculated by MTS, HMTS, and the VODE solver for homogeneous ignition of stoichiometric *n*-decane–air mixture at initial pressure of $P = 1$ atm and initial temperature of $T = 1400$ K. It is seen that both MTS and HMTS agree well with the VODE method for all predictions. The corresponding quantitative comparison of predicted temperature and mass fractions of fuel, CO_2, and OH by VODE, MTS, and HMTS are shown in Table 1

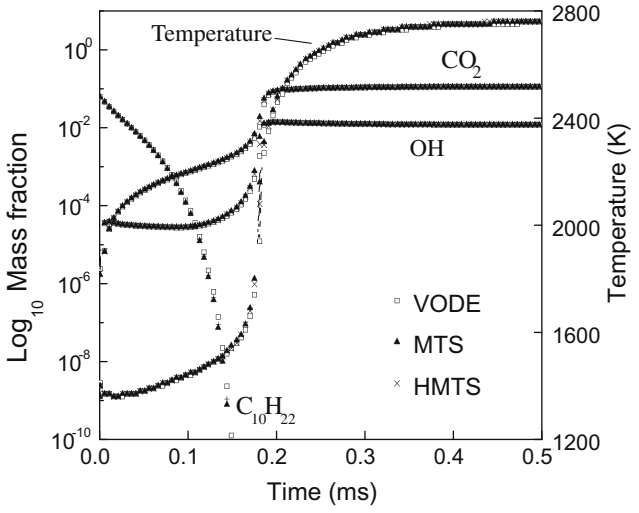

Fig. 5. Time histories of temperature and species mass fractions during ignition predicted by different integration schemes.

at pre-ignition, ignition, and after-ignition times. It is seen that all methods predicted the same equilibrium temperature and species concentrations (converged solution). The maximum differences in temperature and species between the above three methods occurred near ignition due to the slight difference in the predicted ignition delay time. Nevertheless, the maximum difference is within 2% and this difference disappears as the combustion moves towards equilibrium.

To demonstrate the robustness of the HMTS for different selection of species for implicit solutions, the effect of the number of species selected for implicit Euler solutions on the distributions of fuel and OH are shown in Fig. 6a and b, respectively. In Fig. 6a and b, HTMS-1, HTMS-3, and HTMS-5 denote, respectively, that one, three, and five of the fastest groups for implicit Euler integration (see Fig. 3b). Note that each group may have more than one species (see Fig. 2). The results show that the number of implicit groups selected in the HTMS does not affect the distributions of fuel and OH. Similar observation is also observed for other species and temperature distributions. Therefore, from Figs. 5 and 6, we can conclude that the HMTS is robust and accurate. In addition, the number of implicit groups in HTMS can be specified dynamically on each grid and at each time step depending on the level in which the information of time accurate species history is needed.

Fig. 7a shows the comparison of the dependence of ignition delay time on temperature for the stoichiometric *n*-decane–air mixtures at 1 and 20 atmospheric pressures, respectively. The base time step is 0.01 μs. The excellent agreement of MTS and HMTS with the implicit VODE solver demonstrates that both MTS and HMTS are accurate enough (with error less than 1%) to reproduce ignition delay time in a broad temperature range. Fig. 7b shows the comparison of predicted ignition delay time by different models as a function of equivalence ratio. It is also seen that both MTS and HMTS reproduce well the ignition delay time compared to the VODE solver. As shown later, the slight difference (about 1%) comes from the difference in the fixed integration time step in MTS/HMTS while the VODE solver takes a variable integration step.

Fig. 8 shows the comparisons of the normalized CPU time between MTS, HMTS, and the VODE solver for ignition of the stoichiometric *n*-decane–air mixture at 1 atmospheric pressure and different temperatures. It is seen that both MTS and HMTS increases the computation efficiency about one-order in the entire temperature range with the same kinetic mechanism. The HMTS has a slightly better computation efficiency than the MTS. However, it loses the time accurate history of the selected fast modes and has a narrower stability threshold of the base time step than MTS. This is caused by the linear iteration of the implicit solver embedded in the HMTS. Similar results were also obtained for *n*-decane ignition at 20 atm and non-stoichiometric conditions.

For methane–air ignition, Fig. 9a shows the comparison of predicted ignition delay time as a function of initial temperature at 1 and 20 atm for different models. Again, it is seen clearly that both MTS and HMTS agree very well with the VODE solver [6]. The CPU time ratio between MTS/HMTS and VODE solver at 1.0×10^{-8} s base time step is between 0.04 and 0.079, indicating an increase of computation efficiency up to 20 times with the same detailed kinetic model.

For hydrogen–air ignition, Fig. 9b shows the comparison of the predicted ignition delay time of the stoichiometric mixture at 1 atmospheric pressure as a function of the base time step for MTS and VODE solver. Both schemes have the same absolute and relative control errors (see Table 2). The results show that the predicted ignition delay time agrees extremely well at small base time steps. However, as the base time step increases larger than 1 μs, MTS predicted a slightly longer ignition delay time. This difference is due to the fixed integration time step in MTS. In the

Table 1
Quantitative comparison of time histories of temperature, fuel, CO_2, and OH mass fractions predicted by different methods for initial temperature of 1400 K, fuel mass fraction of 0.0614, and pressure of 1 atm (corresponding to Fig. 5).

Time (ms)	Temperature (K)		$C_{10}H_{22}$		CO_2		OH	
0.02	VODE	1360	VODE	0.0215	VODE	6.54e−5	VODE	3.44e−5
	MTS	1360	MTS	0.0214	MTS	6.65e−5	MTS	3.49e−5
	HMTS	1360	HMTS	0.0214	HMTS	6.61e−5	HMTS	3.47e−5
0.2	VODE	2440	VODE	0.0000	VODE	0.0138	VODE	0.0872
	MTS	2470	MTS	0.0000	MTS	0.0139	MTS	0.0893
	HMTS	2460	HMTS	0.0000	HMTS	0.0139	HMTS	0.0887
0.4	VODE	2750	VODE	0.0000	VODE	0.112	VODE	0.0119
	MTS	2750	MTS	0.0000	MTS	0.112	MTS	0.0119
	HMTS	2750	HMTS	0.0000	HMTS	0.112	HMTS	0.0119

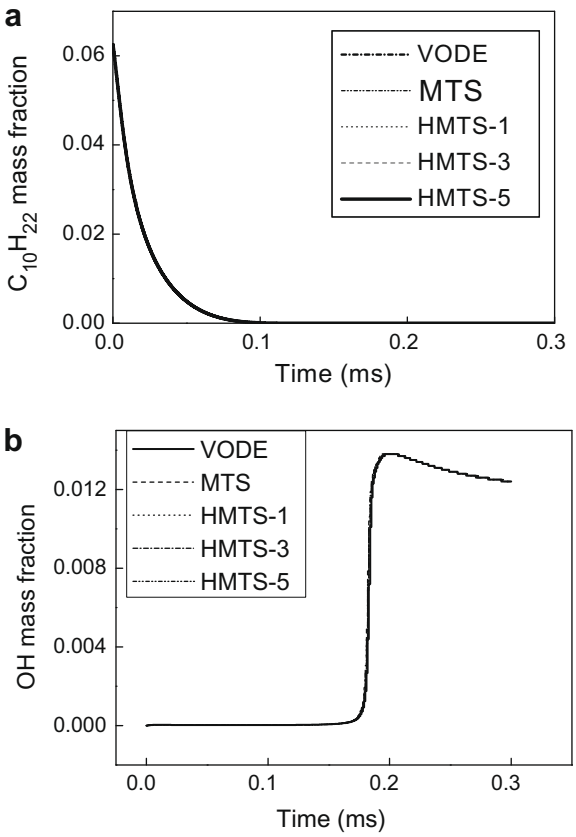

Fig. 6. (a) Effect of the number of selected implicit groups in the HTMS method on the time history of fuel consumption. (b) Effect of the number of selected implicit groups in the HTMS method on the time history of OH.

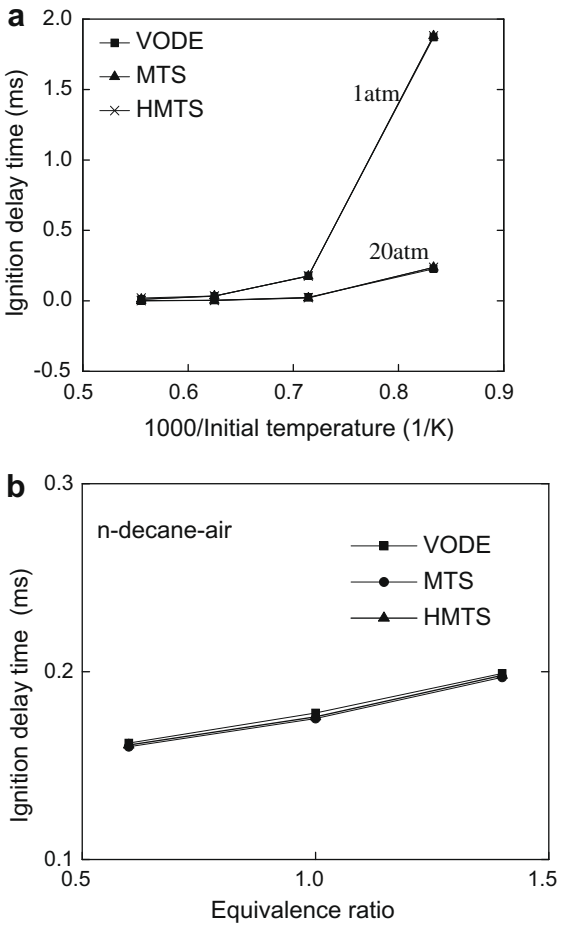

Fig. 7. (a) Ignition delay time as a function of initial temperature for different pressures of stoichiometric *n*-decane–air mixtures. (b) Ignition delay time as a function of equivalence ratio for *n*-decane–air mixtures.

VODE solver, the internal integration time step is dynamically adjusted and a very small time step is used at near ignition. In fact, in most direct numerical simulations the time step is much smaller than 1 μs. In addition, MTS can be simply modified to take a variable integration time steps at ignition conditions to improve the prediction of ignition delay when a large base time step is taken. However, this is not the focus of the present study.

Table 2 shows the comparison of the computation efficiency of the VODE solver and MTS at different base time steps for stoichiometric hydrogen, methane, and *n*-decane–air mixtures. The conventional Euler scheme is not listed here because it is not stable at most calculation conditions. Table 2 shows that with the decrease of the base time step, MTS has an increasing computation efficiency compared to VODE. At the same time, it is also seen that with the increase of the size of the kinetic mechanism, at the same base time step, the relative MTS computation efficiency also increases against VODE. When the MTS method is applied for n-heptane ignition with 160 species, a similar increase of computation efficiency is observed.

3.3. Validation of MTS and HMTS for unsteady propagating flames with detailed and reduced kinetic mechanisms

In order to apply the MTS method to model unsteady flame propagation, we integrated the MTS/HMTS method with the adaptive simulation of unsteady reactive flow code (ASURF) developed at Princeton University by Chen et al. [27]. The code is able to model one-dimensional and two-dimensional unsteady combustion

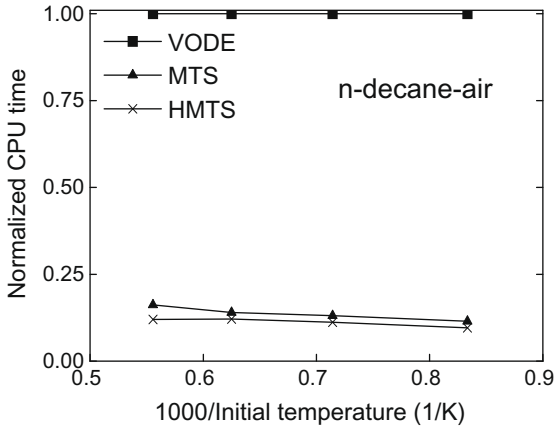

Fig. 8. Comparison of CPU time for *n*-decane ignition for different initial temperatures at 1 atm.

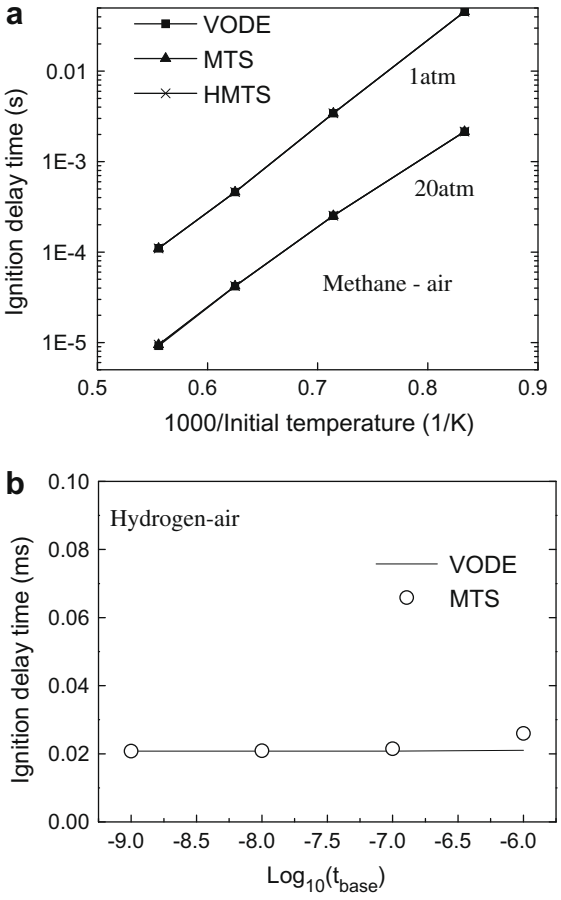

Fig. 9. (a) Comparison of ignition delay time for methane–air mixtures at different pressures. (b) Comparison of ignition delay time for hydrogen–air mixture at different base time steps.

problems with adaptive grids and detailed chemistry. In this paper, we used this code to demonstrate the effectiveness of the MTS/HMTS methods for the modeling of unsteady, outwardly propagating flame using both detailed and reduced kinetic models. The base time step is determined by the acoustic speed and the grid size with CFL = 0.5.

The outwardly propagating, stoichiometric *n*-decane–air spherical flame is initiated at the center in a spherical chamber with an inner diameter of 1 m and pressure of 1 atm by a hot kernel with a radius of 1 mm. The profile of the hot kernel is interpolated from the structure of the corresponding one-dimensional steady state propagating flames. Fig. 10a shows the comparison of the transient flame trajectories (the location of maximum temperature gradient) of stoichiometric *n*-decane/air spherical flame predicted by using HMTS and the implicit VODE solver. The initial acceleration is due to the auto-ignition by the hot kernel. The deceleration of the flame is caused by the diffusion transport and the cooling of the central kernel via thermal diffusion. The acceleration and continuously outward flame propagation is the onset of the quasi-steady spherical flame structure. The comparison in Fig. 10a reveals that the present dynamic multi-timescale algorithm works very well for unsteady flame simulation. Similar to the ignition case, the HMTS significantly reduces the computation time and enables the unsteady flame modeling with a detailed chemistry. On the other hand, the VODE solver is too slow to be used to model the entire spherical flame propagation with a detailed chemistry.

To further increase the computation efficiency, the MTS and HMTS is integrated with a reduced mechanism. In the study, we used a path flux analysis (PFA) based mechanism reduction approach [23] and obtained a reduced *n*-decane mechanism with 54 species from the original detailed mechanism with 121 species and 866 reactions. Fig. 10b shows the evolution of flame trajectories. It is seen also that there is excellent agreement between the HMTS and VODE solver in the simulation of flame trajectory with the reduced mechanism. Moreover, the integration of MTS/HMTS with the PFA generated reduced mechanism decreases the computation time by more than one-order and enables the detailed, unsteady, and adaptive flame modeling of *n*-decane–air flames on a notebook computer within a few hours. Therefore, the integration of the dynamic MTS method with the PFA on-grid model reduction is a promising approach for direct numerical modeling with detailed chemistry. We will address this issue in our future publications.

4. Conclusions

Combustion is a multi-scale problem in nature. An on-grid dynamic multi-time scale (MTS) method and a hybrid multi-time scale (HMTS) method are developed to model multi-timescale combustion problems with detailed and reduced kinetic mechanisms. Comparisons of homogeneous ignition delay time, temperature and species distributions of hydrogen, methane, and *n*-decane–air mixtures in a broad range of temperatures, pressures, and equivalence ratios show that both MTS and HMTS are robust and accurate enough to reproduce the results of the VODE method but can reduce computation time by one-order. The results also show that HMTS has slightly better computation efficiency than MTS but scarifies the stability at larger base time steps. In addition, it is shown that the computation efficiency of multi-time scale method increases with the increase of the kinetic mechanism size and the decrease of base time step. Furthermore, numerical simulations demonstrate that the multi-timescale method does not require accurate estimation of the species timescale and that the present definition of species timescale is consistent with the projected timescale by the CSP method. For the HMTS method, it is also shown that the selection of the species for implicit solutions can be flexible and does not affect the numerical results. Applications of the multi-timescale method to the unsteady flame simulations of outwardly propagating spherical *n*-decane–air flames reveal that the multi-timescale method is promising and computationally efficient for direct numerical simulations of transient combustion processes. The integration of the multi-timescale method with the path flux analysis based mechanism reduction approach

Table 2
Comparison of computation efficiency for calculations of ignition delay time of hydrogen, methane, and *n*-decane air stoichiometric mixtures at different base time steps by using the VODE solver and MTS (detailed mechanism).

No.	Mechanism	Base time step (s)	Initial pressure (atm)	Initial temperature (K)	CPU time (s)		CPU time saving (%)
					VODE	MTS	
a1	H_2	1.0e−6	1	1200	0.28	0.13	53.6
a1	H_2	1.0e−6	1	1200	0.28	0.13	53.6
a2	H_2	1.0e−7	1	1200	2.58	1.31	49.2
a3	H_2	1.0e−8	1	1200	24.9	7.56	69.6
a4	H_2	1.0e−9	1	1200	260	18.4	92.9
b1	CH_4	1.0e−6	1	1400	123	25	79.7
b2	CH_4	1.0e−7	1	1400	1269	181	85.7
b3	CH_4	1.0e−8	1	1400	14,639	1029	93.0
c1	$C_{10}H_{22}$	1.0e−6	1	1400	86	14	83.7
c2	$C_{10}H_{22}$	1.0e−7	1	1400	773	125	83.8
c3	$C_{10}H_{22}$	1.0e−8	1	1400	7609	1049	86.2

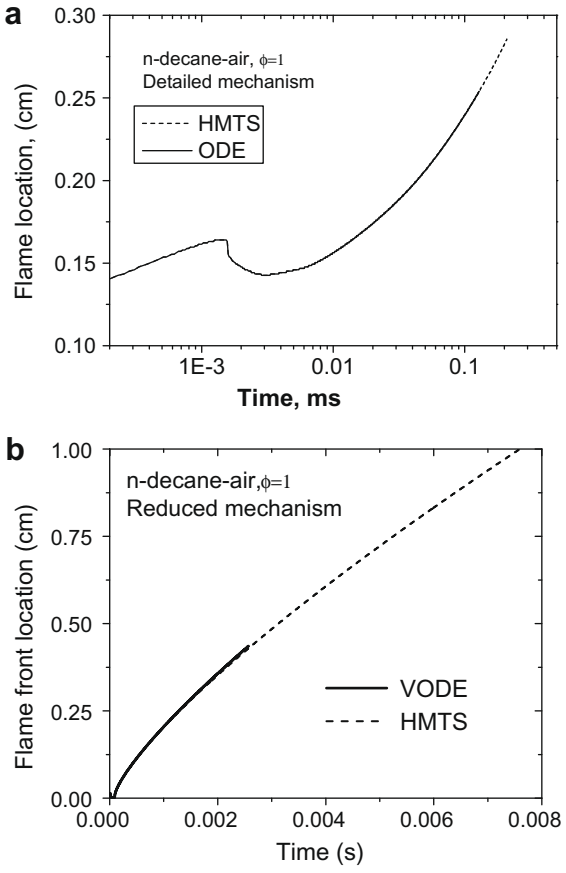

Fig. 10. (a) Comparison between HMTS and VODE solver for the modeling of unsteady spherical flame trajectories of stoichiometric *n*-decane–air mixtures with a detailed mechanism (121 species). (b) Comparison between HMTS and VODE solver for the modeling of unsteady spherical flame trajectories of stoichiometric *n*-decane–air mixtures with a reduced mechanism (54 species).

further demonstrates that a significant increase the computation efficiency can be achieved.

Acknowledgments

This research is jointly supported by the Air Force Office of Scientific Research (AFOSR) MURI research program under the guidance of Dr. Julian Tishkoff and the US Department of Energy, Office of Basic Energy Sciences as part of an Energy Frontier Research Center on Combustion with Grant No. DE-SC0001198.

References

[1] Basic Energy Needs for Clean and Efficient Combustion of 21st Century Transportation Fuels, Basic Energy Sciences Workshop, 2007, US Dept. of Energy. <http://www.science.doe.gov/bes/reports/files/CTF_rpt.pdf>.
[2] W.J. Pitz, N.P. Cernansky, F.L. Dryer, F.N. Egolfopoulos, J.T. Farrell, D.G. Friend, H. Pitsch, AIAA Paper-2007-01-0175, 2007.
[3] E.A. Carter, J.H. Chen, F.L. Dryer, F.N. Egolfopoulos, W.H. Green, N. Hansen, R.K. Hanson, Y. Ju, C.K. Law, J.A. Miller, S.B. Pope, C.J. Sung, D.G. Truhlar, H. Wang, Energy Frontier Research Center for Combustion Science: From Fundamentals to Multi-scale Predictive Models For 21st Century Transportation Fuels, 2009. <http://pcl.princeton.edu/efrc/Personnel.html>.
[4] J. Chen, Petascale direct numerical simulation of turbulent combustion, in: Proceedings of the 6th US National Combustion Meeting, 2009.
[5] T. Lu, C.K. Law, Prog. Energy Combust. Sci. 35 (2009) 192–215.
[6] P.N. Brown, G.D. Byrne, A.C. Hindmarsh, Siam J. Sci. Stat. Comput. 10 (5) (1989) 1038–1051.
[7] D.A. Anderson, J.C. Tannehill, R.H. Pletcher, Computational Fluid Mechanics and Heat Transfer, Hemisphere Publishing, New York, 1984.
[8] N. Peters, Lecture Notes in Physics, Springer, Berlin, 1987.
[9] J.Y. Chen, Combust. Sci. Technol. 57 (1988) 89–94.
[10] Y. Ju, T. Niioka, Combust. Flame 99 (1994) 240–246.
[11] S.H. Lam, Combust. Sci. Technol. 89 (1993) 375.
[12] A. Massias, D. Diamantis, E. Mastorakos, D.A. Goussis, Combust. Flame 117 (1999) 685–708.
[13] T. Lu, Y. Ju, C.K. Law, Combust. Flame 126 (2001) 1445–1455.
[14] U. Maas, S.B. Pope, Combust. Flame 88 (1992) 239.
[15] S.B. Pope, Combust. Theory Model. 1 (1997) 41–63.
[16] S.R. Tonse, N.W. Moriarty, M. Frenklach, N.J. Brown, Int. J. Chem. Kinet. 35 (2003) 438–452.
[17] G. Li, H. Rabitz, J. Hu, Z. Chen, Y. Ju, J. Math. Chem. 43 (3) (2008) 1207–1232.
[18] T. Turanyi, Comput. Chem. 18 (1) (1994) 45–54.
[19] Y. Zhang, R., Rawat, G., Schmidt, Daniel Haworth, Ivana Veljkovic, Paul Plassmann, Acceleration of detailed chemistry calculation in multidimensional engine modeling using DOLFA, in: Proceedings of International Multidimensional Engine Modeling User's Group Meeting, 2005. Detroit, MI. <http://www.erc.wisc.edu/documents/12-Zhang_Multidimensional_New.pdf>.
[20] A.B. Bendtsen, P. Glarborg, K. Dam-Johansen, Comput. Chem. 25 (2001) 161–170.
[21] T. Lu, C.K. Law, Proc. Combust. Inst. 30 (2005) 1333–1341.
[22] P. Pepiot-Desjardins, H. Pitsch, Combust. Flame 154 (2008) 67–81.
[23] Wenting Sun, Zheng Chen, Xiaolong Gou, Yiguang Ju, A path flux analysis method for the reduction of chemical kinetic mechanisms, in: 6th US National Combustion Meeting, Michigan, May 17, 2009, Combustion and Flame, submitted for publication.
[24] E. Hairer, G. Wanner, Solving Ordinary Differential Equations II: Stiff and Differential-Algebraic Problems, Springer, New York, 1996.
[25] C.F. Curtiss, J.O. Hirschfelder, Proc. Natl. Acad. Sci. USA 38 (3) (1952) 235–243.
[26] C.W. Gear, Numerical Initial Value Problems in Ordinary Differential Equations, Prentice-Hall, Englewood Cliffs, NJ, 1971.
[27] Zheng Chen, P. Michael Burke, Yiguang Ju, Proc. Combust. Inst. 32 (2009) 1253–1260.
[28] W. E, B. Engquist, X.T. Li, W.Q. Ren, E. Vanden-Eijnden, Commun. Comput. Phys. 2 (3) (2007) 367–450.
[29] W. E, B. Engquist, Commun. Math. Sci. 1 (1) (2003) 87–132.
[30] B. Engquist, Y.H. Tsai, Math. Comput. 74 (252) (2005) 1707–1742.
[31] W. E, Commun. Math. Sci. 1 (3) (2003) 423–436.
[32] V. Savcenco, W. Hundsdorfer, J.G. Verwer, BIT Numer. Math. 47 (2007) 137–155.
[33] M.S. Day, J.B. Bell, Combust. Theory Modell. 4 (4) (2000) 535–556.

[34] E.S. Oran, J.P. Boris, Numerical Simulation of Reactive Flow, second ed., Cambridge University Press, 2001.
[35] J. Li, Z. Zhao, A. Kazakov, F.L. Dryer, Int. J. Chem. Kinet. 36 (2004) 566–575.
[36] Gregory P. Smith, D.M.G. Michael Frenklach, Nigel W. Moriarty, Boris Eiteneer, Mikhail Goldenberg, C. Thomas Bowman, Ronald K. Hanson, Soonho Song, William C. Gardiner, Jr., Vitali V. Lissianski, Zhiwei Qin GRI-MECH 3.0, <http://www.me.berkeley.edu/gri_mech/>.
[37] M. Chaos, A. Kazakov, Z.W. Zhao, F.L. Dryer, Int. J. Chem. Kinet. 39 (7) (2007) 399–414.
[38] H. Chelliah, Esposito, AIAA Paper-2009-1367, 2009.
[39] T. Turanyi, A.S. Tomlin, M.J. Pilling, J. Phys. Chem. 97 (1993) 163–172.